Small CoFe2O4 magnetic nanoparticles in ferrofluids, influence of the synthesis on the magnetic anisotropies

Niéli Daffé, Véronica Gavrilov, Sophie Neveu, Fadi Choueikani, Marie-Anne Arrio, Amélie Juhin, Philippe Ohresser, Vincent Dupuis, Philippe Sainctavit

Version of Record: https://www.sciencedirect.com/science/article/pii/S0304885318321577
Manuscript_1039f4f98f15193c680009601c25490e

Small $CoFe_2O_4$ magnetic nanoparticles in ferrofluids, influence of the synthesis on the magnetic anisotropies

Niéli Daffé[1,2,3,4], Véronica Gavrilov[2], Sophie Neveu[2], Fadi Choueikani[3], Marie-Anne Arrio[1], Amélie Juhin[1], Philippe Ohresser[3], Vincent Dupuis[2], Philippe Sainctavit[1,3]

[1]Institut de Minéralogie, de Physique des Matériaux et de Cosmochimie, UMR7590, CNRS, UPMC, IRD, MNHN, F-75005 Paris, France.
[2] Sorbonne Universités, UPMC Univ Paris 06, UMR 8234, PHENIX, F-75005 Paris, France.
[3]Synchrotron SOLEIL, L'Orme des Merisiers, Saint-Aubin- BP 48, 91192 Gif-Sur-Yvette, France

***Abstract* — The magnetic properties of cobalt ferrites nanoparticles prepared using three different processes (thermal decomposition, polyol and co-precipitation synthesis routes) are investigated by X-ray Absorption Spectroscopy and X-ray Magnetic Circular Dichroism. The repartition of cobalt and iron ions amongst the interstitial sites of the spinel structure is determined and correlated with their magnetic properties. The study reports on the influence of the synthesis method on the crystallographic order within a nanoparticle, and hence, on the magnetic anisotropy.**

***Keywords:* anisotropies, XMCD, $CoFe_2O_4$, spinel ferrite, nanoparticles.**

1 Introduction

Nanoparticles composed of ferrite nanospinels are used in various applications ranging from medicine to optical devices [1,2]. Among these nanospinels, cobalt ferrite ($CoFe_2O_4$) is a promising material because in the nanosize range it presents a high magneto-crystalline anisotropy energy and a high magnetization saturation. These appealing properties are particularly necessary for hard record devices [3]. For such applications, overcoming the so-called superparamagnetic limit [4] is one of the current biggest challenges. In this direction, various strategies have been developed such as multi-shell structuration [5,6], particle doping [7,8], or coordination of molecules to nanoparticles surfaces [9,10]. However, it is well-known that the preparation route of magnetic nanoparticles can influence in many ways the morphology, their chemical composition or the crystallographic structure which in turn strongly impact the magnetic properties. Among all possible synthesis routes, soft chemical synthesis has become a very convenient way to obtain magnetic ferrite nanospinels. Various synthesis processes have been developed to obtain ferrofluids with long-term stable nanoparticles. In this study we choose three different synthesis that are very common in the preparation of ferrofluids: *(i)* the co-precipitation process is a cost-effective and versatile synthesis that allows to obtain a large amount of nanomaterial [11], *(ii)* the polyol process allows original structures of flower-shaped nanoparticles with enhanced magnetic properties but allows less control on the crystallographic structure [12] and *(iii)* the thermal decomposition route is found to be a very effective method to prepare monodisperse nanoparticles with controlled morphology, although involving higher temperature and more expensive reactants [13]. In the present paper, we investigate the magnetic properties of $CoFe_2O_4$ nanoparticles with diameter ranging between 6 and 7 nm and that have been synthesized by the three different pathways. Correlations between the original effects of a synthesis process on the magnetic properties of $CoFe_2O_4$ nanoparticles obtained has been established by several groups [14–19]. In particular, small spherical $CoFe_2O_4$ nanoparticles synthesized in polyol medium were found to have a saturation magnetization comparable to that of the bulk structure [20,21]. Large coercive field were measured at 5 K on small $CoFe_2O_4$ nanoparticles prepared through high temperature decomposition route: Song and Zhang measured coercive field of 1.1 T on 6 nm $CoFe_2O_4$ nanoparticles [22] and Torres and co-workers measured a coercive field of 1.4 T on 5.7 nm large $CoFe_2O_4$ nanoparticles [23]. In this study, we want to emphasize the fact that magnetic anisotropies of $CoFe_2O_4$ nanoparticles with similar sizes are strongly modulated by the synthesis process. We propose hereby to relate the synthesis routes (co-precipitation, polyol, thermal decomposition) route with the cationic reorganization of the nanoparticles and yielding the observed magnetic properties. Bulk $CoFe_2O_4$ crystallizes in an inverse spinel structure that belongs to the $Fd\bar{3}m$ space group. All Co^{2+} ions occupy octahedral symmetry sites while Fe^{3+} ions are equally distributed between octahedral and tetrahedral symmetry sites [24]. X-ray Magnetic Circular Dichroism (XMCD) at the $L_{2,3}$ edges is a unique tool to probe the 3d magnetic orbitals of the transition elements [25,26]. The method provides a chemical selectivity used to disentangle the magnetic signatures of the cobalt and iron ions. In addition, XMCD is also sensitive to the site symmetry of the absorbing element. The

[4] Present address: *nieli.daffe@psi.ch*. Paul Scherrer Institut, WSLA012, 5232 Villigen PSI, Switzerland

cationic distribution of cobalt and iron between octahedral (O_h) symmetry sites and tetrahedral (T_d) symmetry sites in the nanospinels structures is determined with the investigation of the 6 nm $CoFe_2O_4$ nanoparticles with XMCD. The influence of the synthesis on the crystallographic structure and the magnetic properties of the nanoparticles is thus revealed.

2 Experimental

2.1 *Synthesis*

Co-coprec sample. The cobalt-iron nanospinels Co-coprec were obtained by using a modified Massart process [27]. It consists in precipitating Co^{2+} and Fe^{3+} hydroxydes followed by a heating at boiling temperature to obtain nanoparticles with a meansize of 11 nm. In order to obtain smaller nanoparticles, the Massart process was slightly modified by adding complexing species (tartrate ions) in the mixture of cobalt and ferric nitrates before the addition of sodium hydroxide. The different steps of the synthesis are reported elsewhere [28].

Co-acac sample. Following the route of thermal decomposition of metal precursors developed by Sun *et al.* [13], we have synthesized a second set of small nanoparticles of $CoFe_2O_4$ named Co-acac. The different steps of the so-called "acac" synthesis are reported elsewhere [29].

Co-polyol sample. The third set of small particles of Cobalt-Iron nanospinels is obtained by using the polyol process [30] which consists in a forced hydrolysis of Fe^{3+} and Co^{2+} mixture in a polyol solution. Depending on the polyol used for the synthesis, the morphology of the nanoparticles obtained differs. When the reaction is realized in diethylene glycol (DEG) small spherical nanoparticles are obtained [20].

2.2 *Methods*

Chemical composition of cobalt and iron of the nanoparticles was measured by Atomic Absorption Spectrometry using Perkin Elmer Analyst 100 with an air-acetylene flame at a mean temperature of 2300° C. Table 1 present the ratio of the cationic concentrations of each sample calculated using the molar ratio X_M as detailed in equation (1) below:

$$X_M = [Co]/([Co]+[Fe]) \qquad (1)$$

Nanospinels morphology and size were determined by Transmission Electron Microscopy (TEM) using a JEOL-100 CX2 microscope (UPMC). The analysis of the micrographs of more than 2000 particles leads to size histograms fitted with a log-normal distribution presented in Figure 1.

X-ray Diffraction (XRD) patterns were recorded on the nanoparticles powders using a PANALYTICAL X'Pert Pro MPD diffractometer with the Co Kα radiation ($K_{\alpha 1}$ = 1.79 Å). The size of crystallites domains were calculated on the mean peak (311) using the Scherrer equation [31]. The XRD patterns are presented in Figure 2.

Magnetizations *vs.* magnetic field at 4 K and 300 K have been recorded with a Vibrating Sample Magnetometer (VSM) using a Quantum Design PPMS. Magnetization vs. magnetic field measurements at 4 K were performed on frozen diluted ferrofluid dispersions (Figure 3.) while magnetization curves at 300 K were measured on the nanoparticles powders. The magnetization at saturation (M_S) at 300 K was determined and normalized by the mass of the sample corrected after ThermoGravimetric Analysis. Mass losses of organic species of about 10 % were determined for the Co-acac and Co-polyol samples, and 20 % for the Co-coprec sample. The magnetization at saturation of the nanoparticles at 300 K and the coercive field of the nanoparticles measured at 4 K are presented in Table 1.

X-ray Absorption Spectroscopy (XAS) and XMCD measurements were recorded on the DEIMOS beamline at the French synchrotron facility SOLEIL [32]. XAS and XMCD signals were recorded at the Co and Fe $L_{2,3}$ edges at 4 K under ultra-high vacuum (10^{-10} mbar) in the presence of a 6.4 Tesla magnetic induction. The circularly polarized x-rays are provided by an Apple-II HU52 undulator. The XMCD signals were recorded by flipping both the circular polarization (left and right helicity) and the external magnetic field (either H^+ = + 6.4 T or H^- = – 6.4 T). Each XMCD spectra was thereby acquired by taking the difference:

$$\sigma_{XMCD} = \sigma^- - \sigma^+ \qquad (2)$$

where $$\sigma^- = [\sigma_R(H^+) + \sigma_L(H^-)] \qquad (3)$$

and $$\sigma^+ = [\sigma_R(H^-) + \sigma_L(H^+)] \qquad (4)$$

where σ_L (respectively σ_R) is the absorption cross section measured with left (respectively right) helicity. The measurements were performed on magnetic nanoparticles powders, therefore the XAS spectra were obtained by taking the isotropic absorption cross-section as:

$$\sigma_{XAS} = \frac{\sigma^- + \sigma^+}{2} \qquad (5)$$

XAS and XMCD spectra were normalized by the maximum of the absorption at the L_3 edge.

To extract quantitative determinations of the cationic distributions of the iron-cobalt nanospinels, simulations of the XAS and

XMCD signals were performed using the Ligand Field Multiplet theory developed by Theo Thole [33].The parameters used for the calculations were reported in Hochepied *et al.* [34] for the Co^{2+} ions in $CoFe_2O_4$ and in Carvallo *et al.* [35] for the Fe^{2+} and Fe^{3+} ions in magnetite. The weighted sums of the calculated spectra were fitted to the experimental ones in order to obtain quantitative sites distributions of the Co^{2+} and Fe^{3+} ions among O_h and T_d sites.

3 Results and discussion

3.1 *Size, morphology and chemical composition*

Cobalt-iron nanospinels from the different synthesis routes present similar mean sizes: 6.8 nm for the Co-coprec nanoparticles, 6.7 nm for the Co-acac nanoparticles and 5.6 nm for the Co-polyol nanoparticles and. TEM micrographs show the dependence of the nanoparticles morphology with the synthesis process (Figure 1.). The co-precipitation synthesis leads to non-spherical nanoparticles with a high polydispersity ($\sigma = 0.43$). Nanospinels obtained with the polyol process are spherical but the nanoparticles are highly polydisperse ($\sigma = 0.55$). Cobalt-iron nanospinels synthesized with the acac process are also spherical but the process allows to obtain monodisperse nanoparticles with narrower size distribution ($\sigma = 0.28$). Nanoparticles sizes were also determined by XRD measurements (Figure 2.). The samples present between 30° and 80° (2θ) five peaks that correspond to a spinel structure indexed for $CoFe_2O_4$ (reference code pattern 96-5941-0064) with mean size for coherent domain of 5.4 nm for the Co-coprec nanoparticles, 6.5 nm for the Co-acac nanoparticles and 5.5 nm for the Co-polyol nanoparticles.

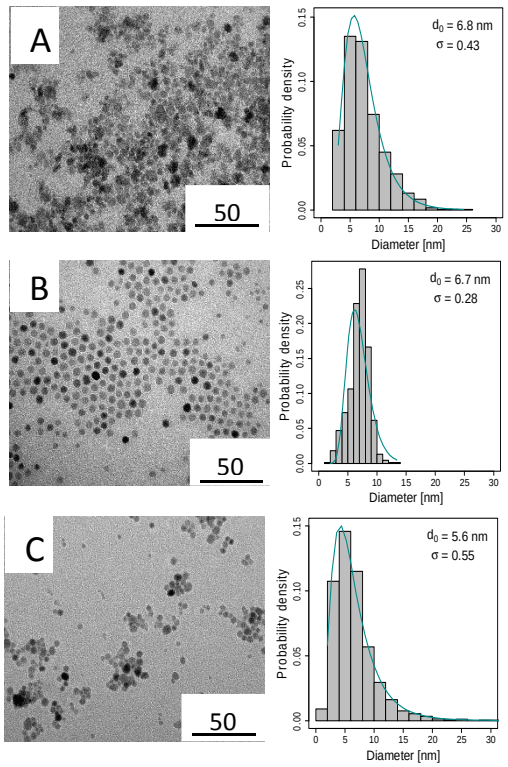

Figure 1. TEM micrographs and size distribution histograms of A) Co-coprec (6.8 nm), B) Co-Acac (6.7 nm) and c) Co-Polyol (5.6 nm) nanoparticles

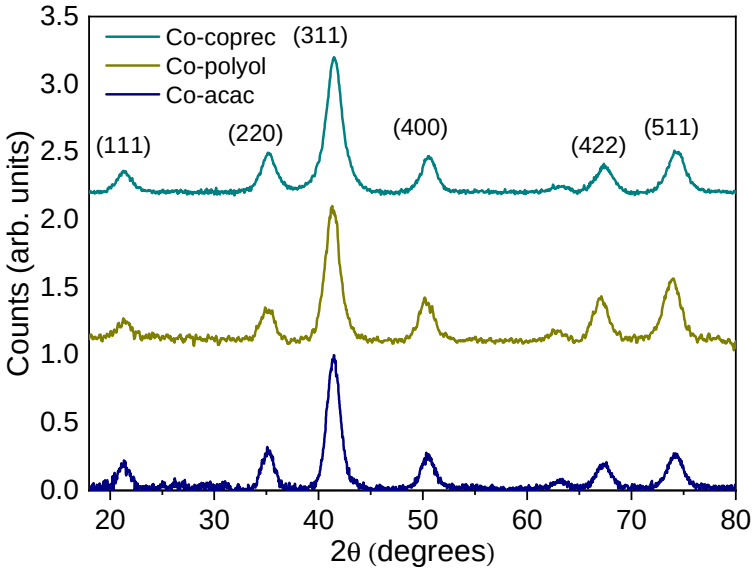

Figure 2- XRD patterns of the Co-acac (blue line), Co-Polyol (dark yellow line) and Co-Coprec (dark cyan line) samples

The X_M value expected for a stoichiometric crystallographic structure of $CoFe_2O_4$ is equal to 33%. From the absorption atomic spectroscopy measurements of Co and Fe concentrations, we obtain lower values of X_M for all cobalt-iron nanospinels obtained. The Co-coprec and Co-acac samples have similar composition with X_M = 26.9 % for the Co-coprec nanoparticles and of X_M = 27.0 % for the Co-acac, while the Co-polyol nanoparticles exhibit a very low molar ratio with X_M = 8.2 %. From XAS at the Fe $L_{2,3}$ edges measured for Co-coprec and Co-polyol, one sees that there is no ferrous iron so that the nanoparticles have to present Vacancies (V) on the octahedral sites. From the values of X_M, the structure of the cobalt-iron nanospinels can be formulated as $Co_{0.79}Fe_{2.14}V_{0.07}O_4$ for the Co-coprec, $Co_{0.81}Fe_{2.19}O_4$ for the Co-acac and as $Co_{0.22}Fe_{2.52}V_{0.26}O_4$ for the Co-polyol nanoparticles.

3.2 ***Magnetometry measurements***

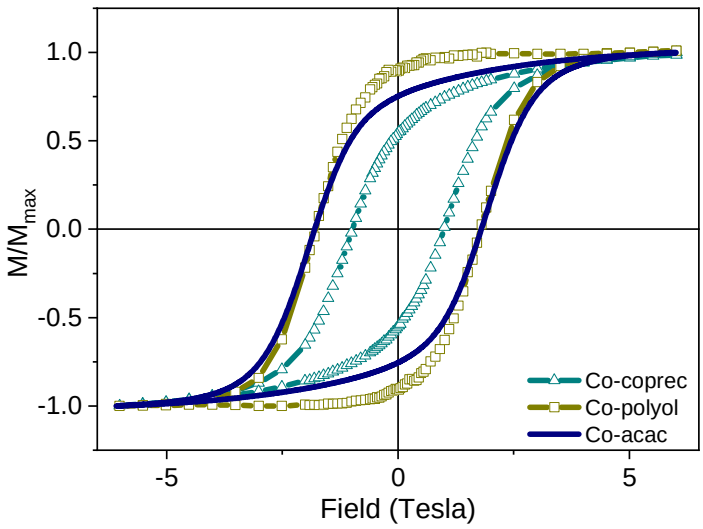

Figure 3. Bulk Magnetization curves measured on ferrofluids samples of Co-acac (blue line), Co-Polyol (dark-yellow square) and Co-Coprec (Dark cyan triangle) at 4 K.

We compare the magnetic properties of the Co-coprec, Co-acac and Co-polyol nanoparticles. The nanoparticles from the different synthesis pathways do not exhibit the same saturation magnetization values M_s (Table 1). The saturation magnetization of the Co-coprec nanoparticles is 66 emu.g^{-1} at 300 K, while the Co-acac and Co-polyol nanoparticles possess lower saturation magnetization of 59 emu.g^{-1} and 51 emu.g^{-1} respectively. The discrepancies of the saturation magnetizations values between the three samples are not surprising considering the different stoichiometries and shapes exhibited by the nanoparticles. The larger value obtain for the Co-coprec can be attributed to the difference of the shape of the nanoparticles which are non-spherical for this sample. Cobalt-iron nanospinels of Co-polyol sample (X_M = 8 %) contain much less cobalt than the Co-acac sample (X_M = 27 %). In addition cobalt-iron nanospinels from the Co-acac contain Fe^{2+} ions which contribute to a higher magnetization. Figure 3 shows the magnetization as a function of the applied magnetic field performed on the frozen phase of the ferrofluid samples (4 K) in zero field cooled. The temperature at which the measurements were performed is well below the blocking temperature of the nanoparticles and the magnetization *vs* applied magnetic field measurements result in magnetic hysteresis curves. The hysteresis curve of the Co-coprec nanoparticles shows a coercive field value of 0.99 T that is twice smaller than that of the Co-acac and Co-polyol nanoparticles. Magnetic coercivities of Co-acac (1.77 T) and Co-polyol (1.8 T) samples are quite similar, but the Co-polyol nanoparticles show a more pronounced remanence ratio than the Co-acac nanoparticles. The remanent magnetization normalized by magnetization at the saturation varies a lot; it is 91% for the Co-polyol, 75% for the Co-acac and 54 % for the Co-coprec sample.

Sample	d_{XRD} nm	d_{TEM} nm	σ_{TEM} nm	X_M %	M_s emu.g^{-1}	H_c T	M_r/M_s	Co^{2+} T_d	Co^{2+} O_h	Fe^{3+} T_d	Fe^{3+} O_h	Fe^{2+} O_h
Co-coprec	5.4	6.7	0.43	26.9	66	0.99	0.54	0.10	0.69	0.86	1.28	-
Co-polyol	5.5	5.6	0.55	8.2	51	1.8	0.91	0.00	0.22	1.00	1.52	-
Co-acac	6.5	6.9	0.27	27	59	1.77	0.75	0.02	0.79	0.98	1.03	0.18

Table 1. Physico-chemicals characteristics of Co-coprec, Co-polyol and Co-acac nanoparticles. d_{XRD} is the particles diameter determined in XRD, d_{TEM} the mean diameter of the nanoparticles measured from TEM micrographs, σ_{TEM} the size distribution, X_M the cationic molar ratio, M_s the saturation magnetization measured at 300 K on the powders nanoparticles, H_c the coercive field measured at 4K on the frozen phase of ferrofluids, M_r/M_s the normalized remanent magnetization, and Co^{2+} T_d, Co^{2+} O_h, Fe^{3+} T_d, Fe^{3+} O_h and Fe^{2+} O_h the occupation of the T_d and O_h sites by the different cations.

3.3 ***XAS and XMCD measurements***

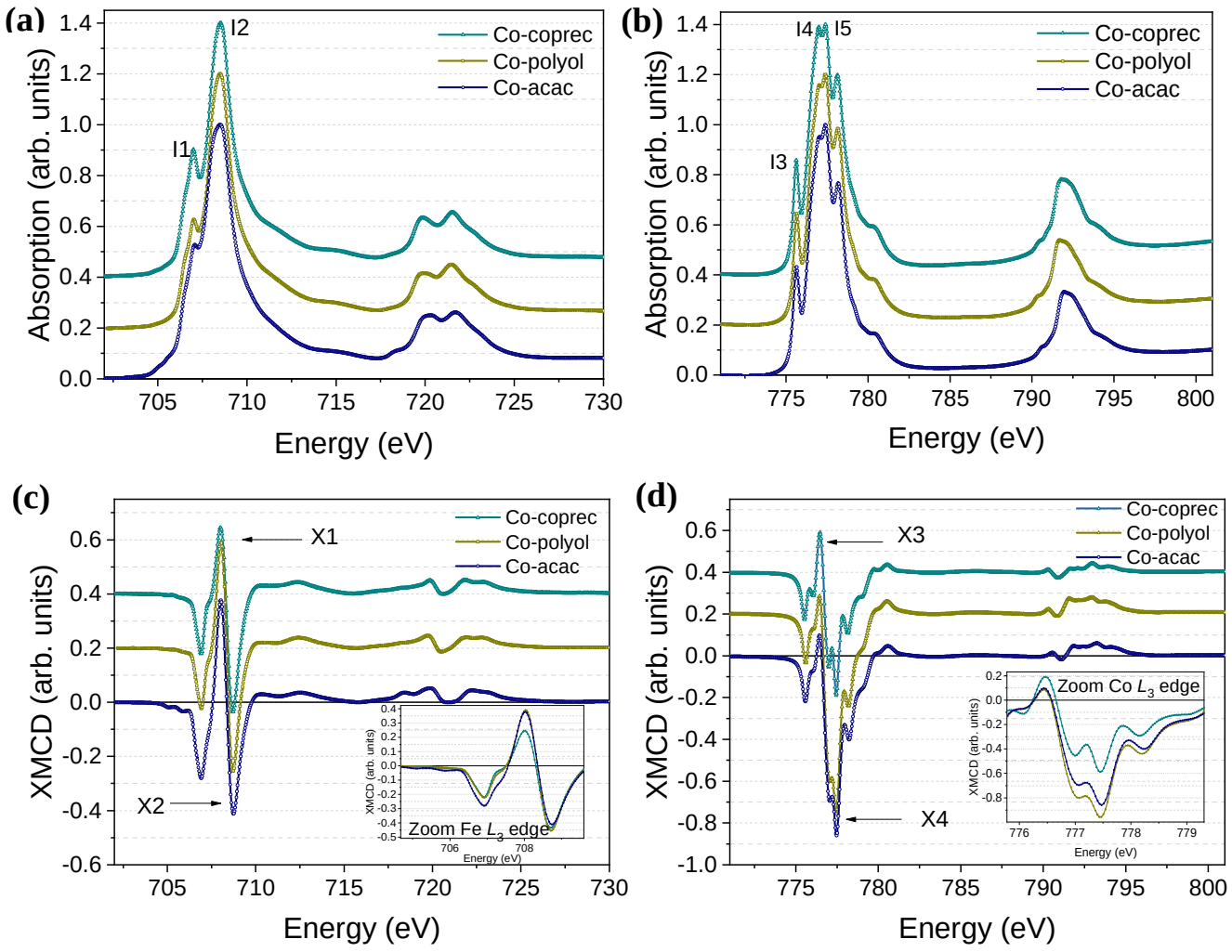

Figure 4. XAS and XMCD spectra measured at 4 K on the dried nanoparticles of Co-coprec (dark cyan triangle), Co-polyol (dark yellow square) and Co-acac (blue circle) samples at the (a) Fe $L_{2,3}$ edges ((a) and (c)) panels) and Co $L_{2,3}$ edges ((b) and (d) panels)

Figure 4. shows the XAS spectra measured at 4 K for the nanoparticles at the Fe $L_{2,3}$ edges (a) and at the Co $L_{2,3}$ edges (b). The XAS spectra are very sensitive to the cationic distribution among the T_d and O_h sites. The magnetic properties investigated with bulk magnetometry measurements can be correlated to the magnetic contributions of the Co and Fe ions in T_d and O_h symmetry sites to the magnetization thanks to element specific XMCD measurements. Indeed, the L_3 edge of the XMCD signals is site sensitive and consists of a positive peak (X1 at 707.98 eV or X3 at 776.41 eV) which can be related to the occupancy of T_d symmetry sites in the case of Fe^{3+} and Co^{2+} respectively, and a negative peak (X2 at 708.69 eV or X4 at 777.51 eV) originating from the cations occupation of the O_h sites symmetry. XMCD spectra measured at the Fe $L_{2,3}$ edges in the Co-coprec and Co-polyol samples are very similar to the one measured in maghemite γ-Fe_2O_3 [36], which contains fully oxidized iron ions Fe^{3+}, while the Fe $L_{2,3}$ edges spectrum for the Co-acac nanoparticles exhibit more intense feature at 705 eV characteristic of the presence of Fe^{2+} ions traces in O_h sites [9] (Figure 4 (c)). At the L_3 edge, XMCD signals display a negative peak when the atomic magnetic moment are parallel to the external magnetic field and a positive peak when the spins are anti-parallel to the external magnetic field. The Fe L_3 edge signals exhibit a X1 peak opposite in sign to the X2 peak, This implies that the magnetic moments of the Fe^{3+} ions in T_d symmetry are coupled antiferromagnetically with the Fe^{3+} ions in O_h symmetry sites. One observes the same trend at the Co L_3 edge where the X3 peak is opposite in sign to the X4 peak.

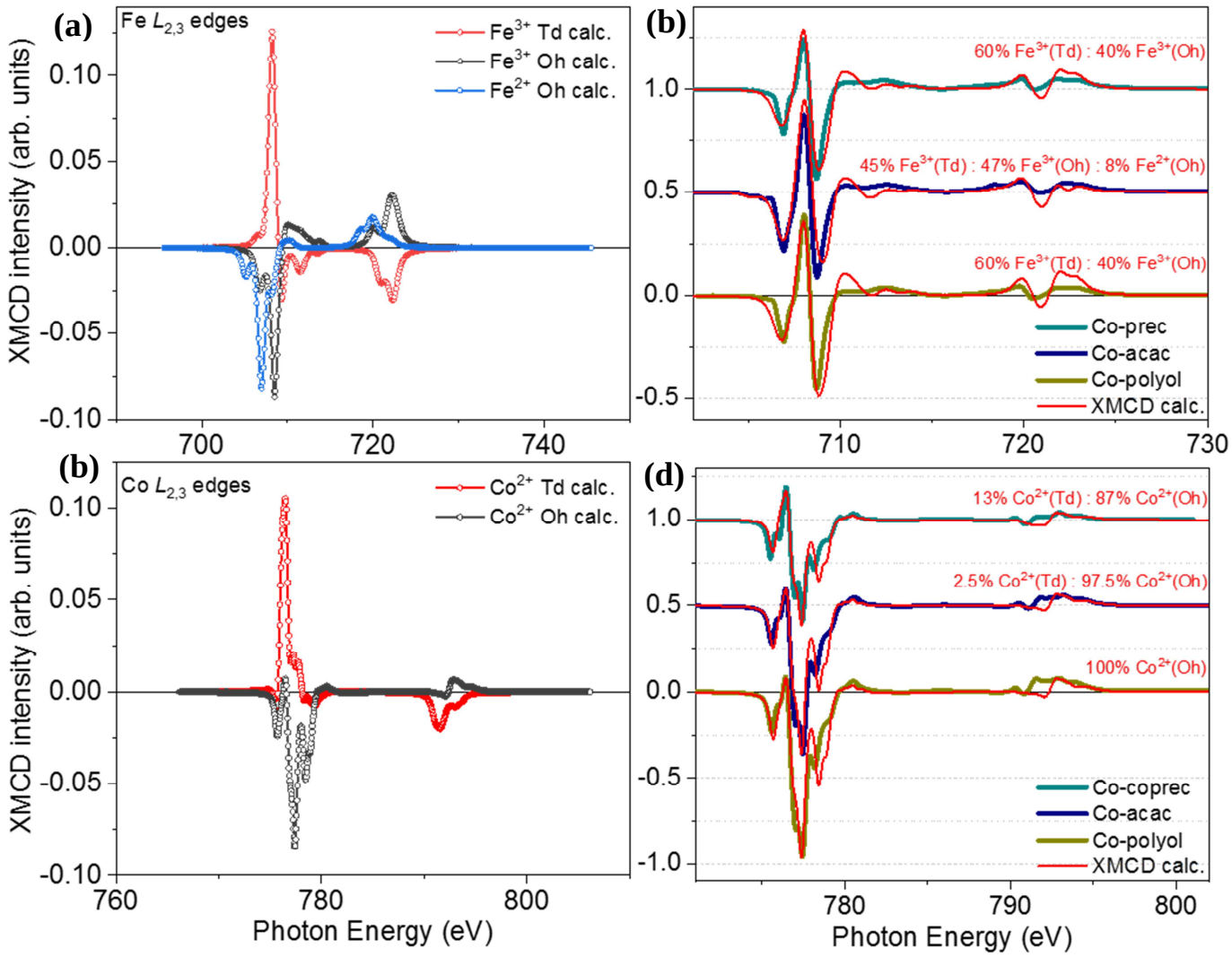

Figure 5. Multiplet calculations of XMCD for Fe^{3+}(Td), Fe^{3+}(Oh) and Fe^{2+}(Oh) ions (panel (a)) and for Co^{2+} (Oh) and Co^{2+}(Td) ions (panel b), along with the weighted averages fitting the experimental XMCD signal at the Fe $L_{2,3}$ edges (panel (b)) and the Co $L_{2,3}$ edges (panel (d)) for the Co-coprec, Co-polyol and Co-acac samples.

From the linear combinations of the calculated XMCD spectra of $Fe^{3+}(O_h)$ and $Fe^{3+}(T_d)$ in the case of the Co-polyol and Co-coprec, and of the $Fe^{2+}(O_h)$, $Fe^{3+}(T_d)$ and $Fe^{3+}(O_h)$ in the case of the Co-acac, one determine the quantitative distribution of the iron in the crystallographic structure (Figure 5 (a) and (b)). The calculated ratio of $Fe^{3+}(T_d)$:$Fe^{3+}(O_h)$:$Fe^{2+}(O_h)$ is 0.98:1.03:0.18 for the Co-acac sample and the calculated ratio of $Fe^{3+}(T_d)$:$Fe^{3+}(O_h)$ is 0.86:1.28 for the Co-coprec nanospinels and 1:1.52 for the Co-polyol nanospinels. The ratio $Fe^{3+}(T_d)$:$Fe^{3+}(O_h)$ expected for a stoichiometric $CoFe_2O_4$ is 1:1. Computational simulations performed in the LFM theory at the Fe^{3+} L_3 edges demonstrates that the distribution of the Fe^{3+} among O_h and T_d symmetry sites is very similar in Co-polyol and Co-coprec samples with 60 % of Fe^{3+} in O_h (40% in T_d) occupation. For the Co-acac nanoparticles, the occupancy of the Fe^{3+} is very close to that of the bulk $CoFe_2O_4$ with 51% of the Fe^{3+} that occupied O_h sites (49% in T_d sites). However, for the Co-acac nanospinels the ratio of the Fe^{2+} ions occupying O_h sites is 8% of the total concentration of iron in the structure. One can observe that this value corresponds approximately to the difference of the O_h occupation of the Fe^{3+} ions between the Co-acac sample and the two others Co-coprec and Co-polyol samples. The lower occupancy of the O_h sites by the Fe^{3+} ions in the Co-acac nanospinels is compensated by the occupation of the O_h sites by the Fe^{2+} ions. The Co $L_{2,3}$ edges spectrum measured in the Co-coprec nanoparticles is typical of a compound containing a mixture of T_d and O_h Co^{2+} [34]. The XMCD signals measured at the Co $L_{2,3}$ edges in the Co-acac and Co-polyol nanoparticles show that in both samples, Co^{2+} ions are predominantly in O_h symmetry with a very intense X4 peak signal (Figure 4 (d)). The XMCD spectra measured fit with the simulated spectra obtained in LFM calculations (Figure 5 (c) and (d)) for a ratio $Co^{2+}(T_d)$:$Co^{2+}(O_h)$ that corresponds to 0.02:0.79 for the Co-acac samples, 0:0.22 for the Co-polyol sample and 0.1:0.69 for the Co-coprec sample. The Co^{2+} ions are all located in O_h sites in the Co-polyol sample, while 2.5% of the Co^{2+} occupied T_d sites in the Co-acac sample. The

inversion degree of the spinel structure of the Co-coprec nanospinels is much lower with 87% of the divalent ion occupancy of O_h symmetry sites (13% of the T_d sites). The magnetic anisotropy of the nanospinels that governs the coercive field measured on the hysteresis loops is consistent with the Co^{2+} ions occupation of the O_h sites. Indeed, the larger occupancy of O_h sites by Co^{2+} coincides with the greater values of coercive field observed with bulk magnetometry measurements (Figure 5.). In the case of nanoparticles prepared with acac and polyol synthesis, the obtained inverse spinel structure with all Co^{2+} ions in O_h symmetry can be interpreted as the result of the high temperature (>200°C) conditions used for the decomposition of the metal precursors in both processes, while the co-precipitation synthesis is carried out at lower temperature (100°C) and the $CoFe_2O_4$ obtained with such softer conditions are metastables.

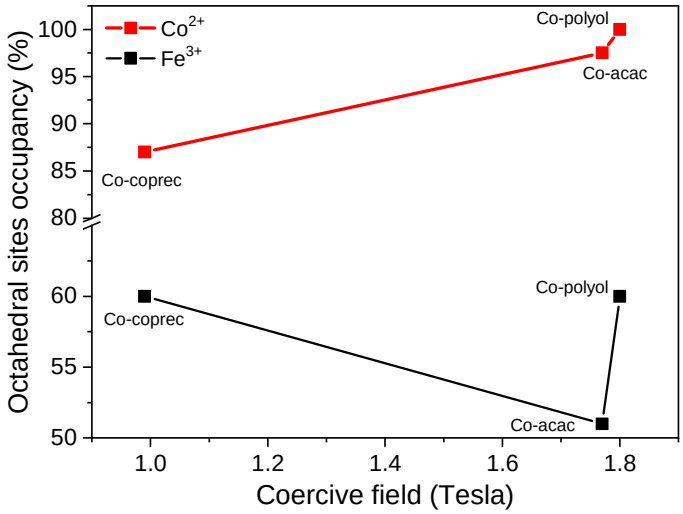

Figure 6. Evolution of the octahedral symmetry sites occupation of Co^{2+} (red square) and Fe^{3+} (black square) with the coercivity. The occupancy of the O_h sites by the metal M, where M is either Co^{2+} or Fe^{3+} is calculated with $M(O_h)/M(total)$.

4 Summary and conclusion

Small magnetic nanoparticles of cobalt-iron nanospinels were obtained through three different synthesis processes. The nanospinels obtained were found to have different chemical compositions, stoichiometries, and shapes. The coercivity measured in the three samples show that the acac and polyol processes allow to obtain nanoparticles with twice larger coercive fields compared to those obtained from the co-precipitation process. XMCD investigations of the nanospinels have provided a quantitative determination of the cationic distribution in the spinel structures. The coercivity is directly related to the presence of Co^{2+} in O_h interstitial sites explaining the enhanced magnetic properties exhibited by the nanoparticles from acac and polyol synthesis. Indeed, on the O_h site Co^{2+} is a Jahn-Teller ion where the spin-orbit coupling and the crystal-field split efficiently the lowest lying levels whereas on the T_d site it is much more symmetrical with minority spin completely occupying the 2-fold degenerated level. Acac and polyol syntheses lead to an increased chemical order, with nanoparticles that have a structure more similar to the bulk structure of $CoFe_2O_4$. In addition, during the acac synthesis some Fe^{2+} ions are formed that also contribute to the magnetic anisotropy.

ACKNOWLEDGMENTS

We thank the organization committee of the conference "*Advances in Magnetics*" held in Bormio, Italy from March 14th to March 16th 2016 where the present paper was submitted and accepted for a presentation. Aude Michel is acknowledged for Atomic Absorption Spectroscopy measurements. We are also grateful to the SOLEIL staff for smoothly running the facilities.

FUNDINGS

This work was supported by French state funds management by the ANR within the Investissements d'Avenir programme under reference ANR-11-IDEX-004-02, and more specifically within the framework of the Cluster of Excellence MATISSE.

CONFLICT OF INTEREST

The authors declare no conflict of interest.

REFERENCES

[1] I. Sharifi, H. Shokrollahi, and S. Amiri, J. Magn. Magn. Mater. **324**, 903 (2012).
[2] F. Choueikani, F. Royer, D. Jamon, A. Siblini, J. J. Rousseau, S. Neveu, and J. Charara, Appl. Phys. Lett. **94**, 051113 (2009).
[3] N. A. Frey, S. Peng, K. Cheng, and S. Sun, Chem. Soc. Rev. **38**, 2532 (2009).
[4] V. Skumryev, S. Stoyanov, Y. Zhang, G. Hadjipanayis, D. Givord, and J. Nogués, Nature **423**, 850 (2003).
[5] J.-H. Lee, J. Jang, J. Choi, S. H. Moon, S. Noh, J. Kim, J.-G. Kim, I.-S. Kim, K. I. Park, and J. Cheon, Nat. Nanotechnol. **6**, 418 (2011).
[6] H. Zeng, J. Li, Z. L. Wang, J. P. Liu, and S. Sun, Nano Lett. **4**, 187 (2004).
[7] G. Salazar-Alvarez, J. Sort, A. Uheida, M. Muhammed, S. Suriñach, M. D. Baró, and J. Nogués, J Mater Chem **17**, 322 (2007).
[8] C. Vichery, I. Maurin, O. Proux, I. Kieffer, J.-L. Hazemann, R. Cortès, J.-P. Boilot, and T. Gacoin, J. Phys. Chem. C **117**, 19672 (2013).
[9] Y. Prado, N. Daffé, A. Michel, T. Georgelin, N. Yaacoub, J.-M. Grenèche, F. Choueikani, E. Otero, P. Ohresser, M.-A. Arrio, C. Cartier-dit-Moulin, P. Sainctavit, B. Fleury, V. Dupuis, L. Lisnard, and J. Fresnais, Nat. Commun. **6**, 10139 (2015).
[10] J. Salafranca, J. Gazquez, N. Pérez, A. Labarta, S. T. Pantelides, S. J. Pennycook, X. Batlle, and M. Varela, Nano Lett. **12**, 2499 (2012).
[11] R. Massart, IEEE Trans. Magn. **17**, 1247 (1981).
[12] P. Hugounenq, M. Levy, D. Alloyeau, L. Lartigue, E. Dubois, V. Cabuil, C. Ricolleau, S. Roux, C. Wilhelm, F. Gazeau, and R. Bazzi, J. Phys. Chem. C **116**, 15702 (2012).
[13] S. Sun, H. Zeng, D. B. Robinson, S. Raoux, P. M. Rice, S. X. Wang, and G. Li, J. Am. Chem. Soc. **126**, 273 (2004).
[14] N. Hanh, O. K. Quy, N. P. Thuy, L. D. Tung, and L. Spinu, Phys. B Condens. Matter **327**, 382 (2003).
[15] E. Manova, B. Kunev, D. Paneva, I. Mitov, L. Petrov, C. Estournès, C. D'Orléan, J.-L. Rehspringer, and M. Kurmoo, Chem. Mater. **16**, 5689 (2004).
[16] S. R. Ahmed, S. B. Ogale, G. C. Papaefthymiou, R. Ramesh, and P. Kofinas, Appl. Phys. Lett. **80**, 1616 (2002).
[17] S. Abramson, V. Dupuis, S. Neveu, P. Beaunier, and D. Montero, Langmuir **30**, 9190 (2014).
[18] V. S. Coker, C. I. Pearce, R. A. D. Pattrick, G. van der Laan, N. D. Telling, J. M. Charnock, E. Arenholz, and J. R. Lloyd, Am. Mineral. **93**, 1119 (2008).
[19] J. M. Byrne, V. S. Coker, S. Moise, P. L. Wincott, D. J. Vaughan, F. Tuna, E. Arenholz, G. van der Laan, R. a. D. Pattrick, J. R. Lloyd, and N. D. Telling, J. R. Soc. Interface **10**, 20130134 (2013).
[20] S. Ammar, A. Helfen, N. Jouini, F. Fiévet, I. Rosenman, F. Villain, P. Molinié, and M. Danot, J. Mater. Chem. **11**, 186 (2001).
[21] M. Artus, L. B. Tahar, F. Herbst, L. Smiri, F. Villain, N. Yaacoub, J.-M. Grenèche, S. Ammar, and F. Fiévet, J. Phys. Condens. Matter **23**, 506001 (2011).
[22] Q. Song and Z. J. Zhang, J. Am. Chem. Soc. **134**, 10182 (2012).
[23] T. E. Torres, A. G. Roca, M. P. Morales, A. Ibarra, C. Marquina, M. R. Ibarra, and G. F. Goya, J. Phys. Conf. Ser. **200**, 072101 (2010).
[24] Y. H. Hou, Y. J. Zhao, Z. W. Liu, H. Y. Yu, X. C. Zhong, W. Q. Qiu, D. C. Zeng, and L. S. Wen, J. Phys. Appl. Phys. **43**, 445003 (2010).
[25] F. M. F. de Groot, J. Electron Spectrosc. Relat. Phenom. **67**, 529 (1994).
[26] G. van der Laan, E. Arenholz, R. V. Chopdekar, and Y. Suzuki, Phys. Rev. B **77**, 064407 (2008).
[27] F. A. Tourinho, R. Franck, and R. Massart, J. Mater. Sci. **25**, 3249 (1990).
[28] N. Daffé, F. Choueikani, S. Neveu, M.-A. Arrio, A. Juhin, P. Ohresser, V. Dupuis, and P. Sainctavit, J. Magn. Magn. Mater. (n.d.).
[29] V. Gavrilov-Isaac, S. Neveu, V. Dupuis, D. Taverna, A. Gloter, and V. Cabuil, Small **11**, 2614 (2015).
[30] D. Caruntu, G. Caruntu, Y. Chen, C. J. O'Connor, G. Goloverda, and V. L. Kolesnichenko, Chem. Mater. **16**, 5527 (2004).
[31] P. Scherrer, Nachrichten Von Ges. Wiss. Zu Gött. Math.-Phys. Kl. **1918**, 98 (1918).
[32] P. Ohresser, E. Otero, F. Choueikani, K. Chen, S. Stanescu, F. Deschamps, T. Moreno, F. Polack, B. Lagarde, J.-P. Daguerre, F. Marteau, F. Scheurer, L. Joly, J.-P. Kappler, B. Muller, O. Bunau, and P. Sainctavit, Rev Sci Instrum **85**, 013106 (2014).
[33] B. T. Thole, G. van der Laan, J. C. Fuggle, G. A. Sawatzky, R. C. Karnatak, and J.-M. Esteva, Phys. Rev. B **32**, 5107 (1985).

[34] J. F. Hochepied, P. Sainctavit, and M. P. Pileni, J. Magn. Magn. Mater. **231**, 315 (2001).
[35] C. Carvallo, P. Sainctavit, M.-A. Arrio, N. Menguy, Y. Wang, G. Ona-Nguema, and S. Brice-Profeta, Am. Mineral. **93**, 880 (2008).
[36] S. Brice-Profeta, M.-A. Arrio, E. Tronc, N. Menguy, I. Letard, C. Cartier dit Moulin, M. Noguès, C. Chanéac, J.-P. Jolivet, and P. Sainctavit, J. Magn. Magn. Mater. **288**, 354 (2005).